ingegneria sismica
International Journal of Earthquake Engineering
Anno XLIII - Num. 1 - 2026

Ultrasonic imaging optimization of cable lead seal defects based on filtering interpolation

Jianfeng Wu[1], *Hai Zheng*[1], *Qingdong Zhou*[1], *Zhiming Zhen*[1,*], *Jichen Wang*[1] *and Zhiguo Ni*[1]

[1] Jiangmen Power Supply Bureau, Guangdong Power Grid Co., Ltd., Jiangmen, Guangdong 529000, China

SUMMARY: *When employing ultrasonic phased array sector scanning technology to detect defects in the lead seal of cable terminals, the irregular surface of the lead seal often prevents complete contact with the probe. This misalignment results in imaging issues such as noise, artifacts, and discontinuous defect representations. To address these challenges, a novel method for enhancing the quality of ultrasonic images of lead seal defects has been developed. The process begins with filtering and denoising the fan-scan image data of lead seal defects gathered from phased array equipment. Subsequently, the denoised data undergoes enveloping via the Hilbert transform, followed by interpolation using the Lanczos method. The refined image data is then subjected to angle correction before final imaging. Experimental comparisons demonstrate that this method effectively eliminates noise and artifacts from the fan-scan images of lead seal defects. Specifically, the signal-to-noise ratio of the threshold filter image surpasses that of the median and mean filters by 6.28 dB and 6.07 dB, respectively. Additionally, the continuity of the defect edges is significantly enhanced. These improvements in imaging quality facilitate more accurate detection and quantification of lead seal defects.*

KEYWORDS: *Cable termination; Lead seal; Fan scan image; Denoising; Lanczos interpolation*

1 Introduction

High-voltage cables play a critical role in power transmission, and their safe operation is essential for the stability of the power system [1]. The lead seal, as a key component for connecting and sealing high-voltage cable terminals, is prone to defects such as cracks, holes, or deformations due to improper installation or continuous mechanical stress and vibration during operation. These defects can compromise the sealing and connection performance of the lead seal, leading to moisture ingress, poor electrical connections, and reduced insulation levels. Consequently, such issues may trigger tripping incidents in high-voltage cable lines, jeopardizing the operational safety of the power grid [2, 3]. Therefore, exploring defect detection methods for lead seals in cable accessories holds significant practical importance.

Currently, various non-destructive testing methods are available for lead seal defects. For instance, X-ray detection relies on the electrical signals generated by X-rays penetrating the lead seal to assess its condition [1]. The loop resistance method evaluates the lead seal's state by measuring changes in its electrical resistance. Eddy current testing detects lead seal conditions by monitoring variations in cable impedance and voltage [4]. However, these methods are often limited by their operational complexity, stringent detection requirements, and

*472895899@qq.com
https://doi.org/10.65102/is20261023
Published: 30 April, 2026

time-consuming procedures, making them impractical for convenient and reliable detection of lead seal defects in cable terminals.

Fang Chunhua et al. [3] proposed the use of ultrasonic phased array technology for detecting lead seal defects. This method identifies defect locations based on the time and amplitude of defect echoes, offering simplicity and high detection efficiency, making it an effective approach for lead seal defect detection. Among ultrasonic phased array techniques, sector scanning imaging stands out due to its wide detection range, intuitive image display, and straightforward detection conditions. Compared to conventional ultrasonic methods, it is better suited for inspecting areas with limited scanning contact [5-8]. Thus, ultrasonic sector scanning imaging is particularly suitable for lead seal defect detection.

However, when ultrasonic phased array sector scanning is applied to lead seal defect detection, challenges arise due to the incomplete contact between the phased array probe and the curved surface of the lead seal. Even with the application of coupling agents, beam divergence occurs, leading to noise in the echo signals and artifacts in the imaging. Additionally, misalignment in echo data during angle transformation imaging results in discontinuous edges of lead seal defects. These issues hinder the accurate detection and quantification of lead seal defects, necessitating further improvements in the quality of ultrasonic sector scanning imaging.

Researchers worldwide have extensively studied the problems of noise, artifacts, and discontinuous defect edges in ultrasonic imaging. Liu Yuanyu [9], while investigating the ultrasonic identification of micro-defects, proposed a wavelet threshold denoising method that preserves the main signal components while effectively removing noise, enabling precise identification of micro-defects. Dai Yanqing [10] explored various threshold denoising algorithms to effectively eliminate noise from noise-contaminated images. In 2017, Hadi Ghasemifard et al. [11] demonstrated that processing ultrasonic radiofrequency data with threshold algorithms before imaging could effectively reduce noise and artifacts. Yang Xiuqing [12] suggested applying Lanczos interpolation to ultrasonic image data before iterative back-projection reconstruction, smoothing the interpolated digital signal values and enhancing imaging quality at defect locations. However, none of these studies specifically addressed the optimization of ultrasonic sector scanning images for lead seal defects in high-voltage cable accessories. This paper further investigates the ultrasonic sector scanning image data of lead seal defects to address noise, artifacts, and discontinuous defect edges.

This paper proposes a filtering and interpolation-based optimization method for improving the quality of ultrasonic sector scanning imaging of high-voltage cable lead seals. The method addresses issues such as artifacts, noise, and blurred or discontinuous defect shapes in images obtained using ultrasonic phased array sector scanning. The proposed approach sequentially applies filtering, Hilbert envelope extraction, and Lanczos interpolation to the image data, aiming to enhance imaging quality by providing high signal-to-noise ratio data. Experimental validation confirms the feasibility of this optimization method for improving the quality of ultrasonic sector scanning imaging of high-voltage cable lead seals.

2 Ultrasound phased-array fan-scan imaging principle

The process of ultrasonic phased array sector scanning imaging begins with the pulse transmitter exciting all elements of the transducer at different delay times, causing each element to emit ultrasonic waves. During propagation, these waves superimpose and synthesize to achieve deflection and focusing at specific positions. When the piezoelectric phased array probe emits deflected and focused ultrasonic waves, the synthesized beam generates reflected waves upon encountering defects such as cracks or holes in the lead seal. All elements then act as

receiving transducers to capture the reflected defect echo signals. These echo signals undergo delay-and-sum processing to obtain a sequence of echo signals at a specific deflection angle. The workflow of ultrasonic phased array transmission and reception is illustrated in Figure 1.

During the delay-and-sum processing of echo data, since the echo signals exist as sampled points, the delay is implemented by adding corresponding points to the echo data. By summing the received data from all elements at a specific angle, the delay-and-sum data for that angle can be obtained.

Phased array sector scanning involves scanning at different angles within a defined angular range with equal angular steps. Assuming there are n equally spaced scan lines and m echo signal data points at each angle, the echo data from each scan line are sequentially arranged into a matrix, forming an m×n matrix that constitutes the raw image data [5]. This image data is then subjected to coordinate transformation and correction to convert it into real-world coordinate data. Finally, the data is displayed in a rectangular image as a sector-shaped region, thereby achieving phased array sector scanning imaging [5].

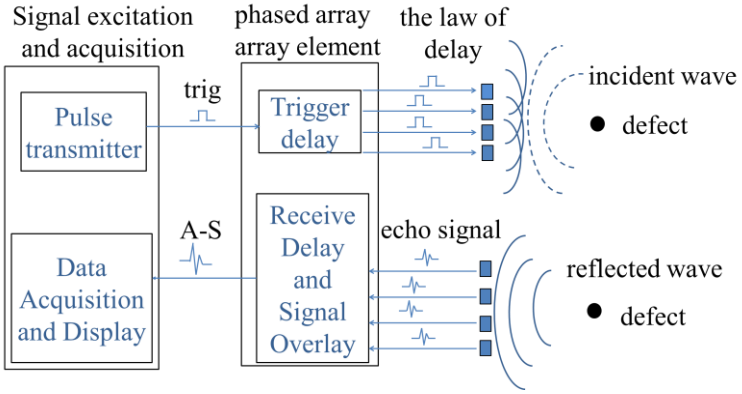

Figure 1: Flow of ultrasonic phased array transmitting and receiving sound waves

3 Optimization of fan-scan imaging quality for ultrasonic inspection of lead seals

3.1 Analysis of fan-scan images of seal defects obtained by phased array equipment

When the phased array equipment is used to detect seal defects, a fan-scan image of seal defects will appear as shown in Figure 2(a), from which seal defects can be clearly seen, but there are very serious artifacts as well as noise around the defects, as shown in the box in Figure 2(a), which will affect the judgment of seal defects and pseudo defects.

Based on the experimental experience, when trying to repeatedly move the position of the probe, adjusting the pulse width, and adjusting the focal length, the results were obtained as shown in Figure 2(b), Figure 2(c), and Figure 2(d). From the figure, it can be seen that there are still very serious artifacts and background noise near the defects, so simply moving the probe and changing the phased array parameters cannot effectively improve the noise and artifacts in the fan-scan image of the seal defects.

When we use phased array equipment to detect lead seal defects, a sector-scan image of lead seal defects as shown in Figure 1(a) will appear. The lead seal defects can be clearly seen from the picture, but there are very serious artifacts around the defects. and background noise are shown in the box in Figure 1(a), which will affect our judgment of lead seal defects and

pseudo-defects.

When an attempt was made to move the position of the probe repeatedly to eliminate artifacts and background noise caused by improper experimental operation, the result shown in Figure 1(b) was obtained. From the picture, we can see that there are still very serious artifacts and background noise near the defect, which proves that simply moving the probe cannot effectively improve the noise and artifacts in the sector-scan image of lead seal defects.

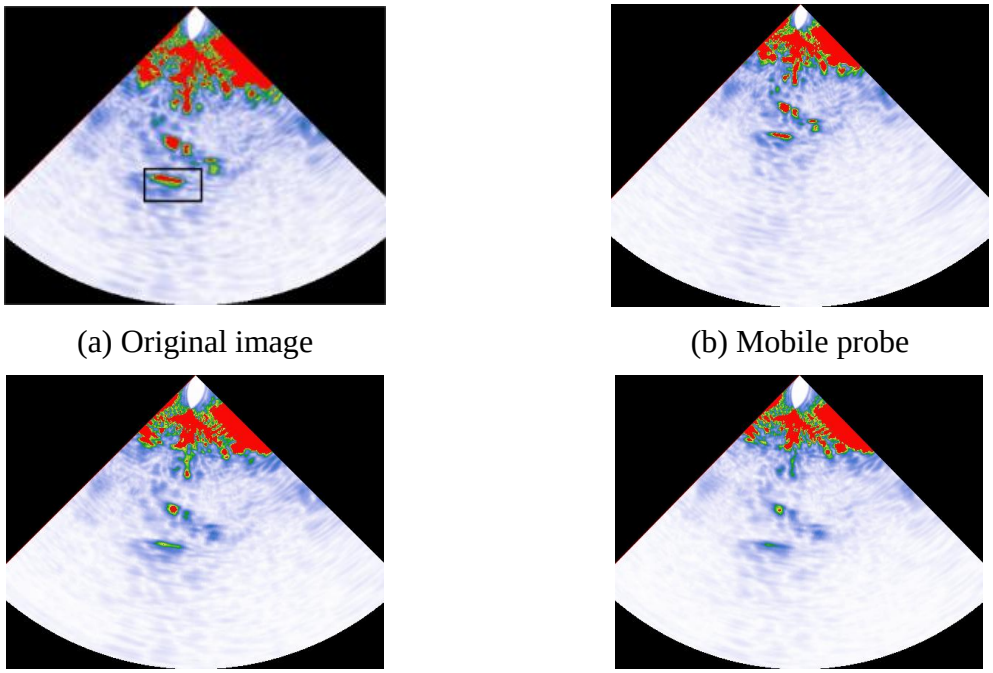

(a) Original image (b) Mobile probe

(c) Change pulse width (d) Change Depth of Focus

Figure 2: Ultrasound images of seal defects

After verifying the effect of experimental conditions on noise, the next step is to optimize the quality of fan-scan imaging of cable terminal lead seal defects from the perspective of data processing, i.e., to collect the fan-scan image data of the lead seal defects received by the phased array equipment, and to process the data into data with a high signal-to-noise ratio before imaging.

3.2 Quality optimization process for fan-scan imaging of cable termination lead seal defects

In order to filter out the background noise as well as the artifacts in the phased-array fan-scan image of the cable terminal seals and to improve the imaging quality, the phased-array fan-scan image data of the defective cable terminal seals are sequentially filtered, Hilbert transformed, and Lanczos interpolated before the angle-corrected imaging to improve the signal-to-noise ratio. The specific process is shown in Figure 3:

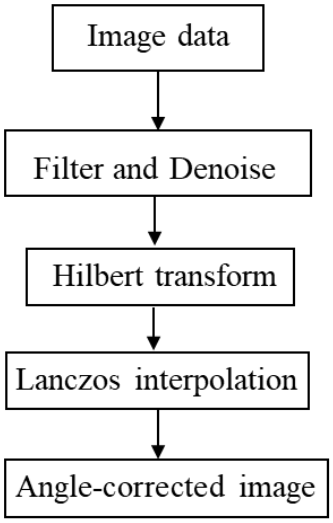

Figure 3: Quality optimization process for fan-scan imaging of cable termination lead seal defects

3.2.1 Seal fan-scan image data filtering and denoising

Ultrasonic phased array detection of seal defects is affected by the shape of the seal surface, probe, etc., and is prone to produce background noise and artifacts that are not defective echoes, reducing the reliability of the detection results. For this purpose, some filtering denoising methods are introduced to remove the noise.

(1) Median filtering is a nonlinear signal processing technique that replaces the value of a point in the image matrix data with the median value of its neighboring data points, thereby eliminating isolated noise points [13].

The formula for median filtering of image data is as follows:

$$l(x,y) = mid\left\{ f(x-k, y-l), (k,l \in M) \right\} \tag{1}$$

where (x,y) is the location where the image data is located, $f(x,y)$, $l(x,y)$ are the magnitude of the original image and the processed image data at (x,y), respectively. M is a two-dimensional sliding template, which is usually in the shape of a square with the size of 5×5.

(2) Mean filtering is a simple and easy to perform linear filtering, the basic idea is to take the mean value of the window image data as the output value at the center position. Mean value filtering has strong denoising ability and fast speed, which is widely used in image processing[13].

Its mathematical formulation for the mean filtering of the image data located at (x,y) is expressed as:

$$f' = \frac{\sum_{i=1}^{|M|} f(x,y)}{|M|} \qquad (x,y) \in M \tag{2}$$

where M is a sliding window, $|M|$ is the size of the window, that is, the amount of data contained in the window, (x,y) is the location of the image data, $f(x,y)$ is the processed image data

amplitude at matrix (x, y).

(3) Analysis of the fan-scan image data of the seal defects shows that the data values at the defects are the largest, the data at the noise are in the middle segment of values, and the data at the absence of background noise are the smallest. By setting the threshold amount, the data at the seal defects and the data at the absence of noise are retained and the data at the noise is filtered out[14].

The optimal threshold for filtering out the noise is calculated by the maximum interclass variance algorithm OTSU. The principle is that when the interclass variance between defective and noisy data is larger, the difference between defective and noisy is also larger, and then the noise can be effectively removed by threshold filtering[15]. Therefore by finding the threshold value that maximizes the interclass variance between the defects and the noise is used as the optimal threshold value. The derivation process to obtain the optimal threshold is as follows:

Let there be L numerical quantities in the image data, N_i data of size i, and a total of N numbers in the matrix, then the percentage of each data is:

$$P_I = \frac{N_{\mathrm{i}}}{N} \tag{3}$$

where i ranges from 1 to , then the mean value of the image data is:

$$\mu_T = \sum_{i=0}^{L-1} iP_i \tag{4}$$

Assuming that is the threshold for filtering out noise, let $\omega_0(T)$ and $\omega_1(T)$ be the ratio of the data at the seal defects and the noise data respectively, then the average value of the data at the defects and the noise data is:

$$\omega_0(T) = \frac{\sum_{i=0}^{T} iP_i}{\omega_0(T)} \tag{5}$$

$$\omega_1(T) = \frac{\sum_{i=T+1}^{L-1} iP_i}{\omega_1(T)} \tag{6}$$

This shows that the interclass variance between the data at the defect and the noise data is:

$$\sigma^2(T) = \omega_0(T)\left[\mu_0(T) - \mu_T\right]^2 + \omega_1(T)\left[\mu_1(T) - \mu_T\right]^2 = \omega_0(T) \times \omega_1(T) \tag{7}$$

In OSTU method, the threshold that maximizes the inter-class variance is the optimal threshold for filtering out the background noise with the expression:

$$\sigma^2(T^*) = \max_{0 \le T \le L-1} \left\{\sigma^2(T)\right\} \tag{8}$$

Similarly, the optimal threshold for retaining a noise-free background was calculated using the OTSU algorithm.

Based on the above calculation, it can be made that T_1 is the optimal threshold for filtering out the noise and T_2 is the optimal threshold for retaining the noise-free background. The

principle of threshold de-noising is:

$$f^{'}(x,y)=\begin{cases} f(x,y) & f(x,y)\geq T_1 \\ T_2 & T_2<f(x,y)<T_1 \\ f(x,y) & f(x,y)<T_2 \end{cases} \tag{9}$$

In the above equation, the $f(x,y)$ is the image data to be processed, $f^{'}(x,y)$ is the image data after threshold de-noising.

In this paper, the optimal parameters of each filtering algorithm are taken to perform the fan-scan imaging experiments, and its parameters are set as shown in Table 1.

Table 1: Optimal parameterization of the comparison algorithm

Arithmetic	Optimal parameterization
median filter	window size:5×5
mean value filter	window size:10×10
threshold filtering	threshold:170, 10

3.2.2 Hilbert Transform of Seal Fan-Scan Image Data

When ultrasound fan-scan image data is threshold filtered, a lot of noise can be removed. However, after threshold filtering, the imaging after angular correction will show that the edges of the fan-scan image are weakened, the left and right edges disappear, and the image resolution is reduced. To address this phenomenon, a radially symmetric Hilbert transform is introduced, which enhances the 2D edges of the fan-scanned image and improves the resolution[16, 17].

3.2.3 Lanczos Interpolation of Seal Fan-Scan Image Data

When the ultrasonic fan-scan image data is directly imaged after filtering and denoising, and the Hilbert transform takes the envelope, it will appear that some data point positions in the image cannot be matched with the transformed positions, which directly leads to the cloudy appearance of the defects of the lead seals, which seriously reduces the recognition of the defect edges. To solve this problem, the image data is interpolated. The interpolation process will result in invalid data being effectively filled and valid data being fully utilized, which in turn improves the contrast of the fan-scan image of the lead seal defect.

Lanczos interpolation which has low computational complexity, gives better image quality and is suitable for real time scaling of color images is selected after the study[12]. The principle of Lanczos interpolation is to perform convolution operation on the image data. The most critical aspect of Lanczos interpolation is to choose out the kernel function and interpolation parameters.

The kernel function formula is as follows:

$$L(x)=\begin{cases} \sin c(x)\sin c(x/a), & if\ -a<x<a \\ 0, & otherwise \end{cases} \tag{10}$$

or

$$L(x)=\begin{cases}1 & if\ x=0\\ \dfrac{a\sin(\pi x)\sin(\pi x/a)}{\pi^2x^2} & if\ -a\le x\le a\ and\ x\ne 0\\ x & otherwise\end{cases} \tag{11}$$

where a is the width of the kernel function, i.e., the interpolation parameter, which is set to 3 here.

The process of Lanczos interpolation is as follows: first determine the location of the interpolation point and take a window in the original image with the interpolation point as the center.Then for each image data in the window, its weight is calculated using Lanczos kernel function. Finally, the weights of all the image data in the window are multiplied with the interpolated values to get the final values of the interpolated points.

After the seal defect fan-scan image data is processed as described above, it has to be mapped to a different color in order to improve the image contrast. Depending on the size of the image data, blue green red is presented in order from low to high.

4 Experimental comparison

4.1 Experimental platform construction

The feasibility of the imaging optimization scheme in this paper is next verified experimentally. Cable terminal lead seal real picture and defects schematic diagram shown in Figure 4 (a), experiments using manually produced lead seal hole defects shown in Figure 4 (b), ultrasonic phased array detection of lead seal defects fan scanning imaging experimental platform shown in Figure 4 (c). Ultrasound phased array equipment selected 16 array elements of one-dimensional phased array probe, the length of the array element 10mm, the center of the array element spacing is 1mm, the sampling frequency is 100MHz. Through the analysis in 2.1, the parameters of the device are selected for the best imaging effect of the lead seal defects, in which the pulse width is 180ns and the aggregation depth is 11mm.

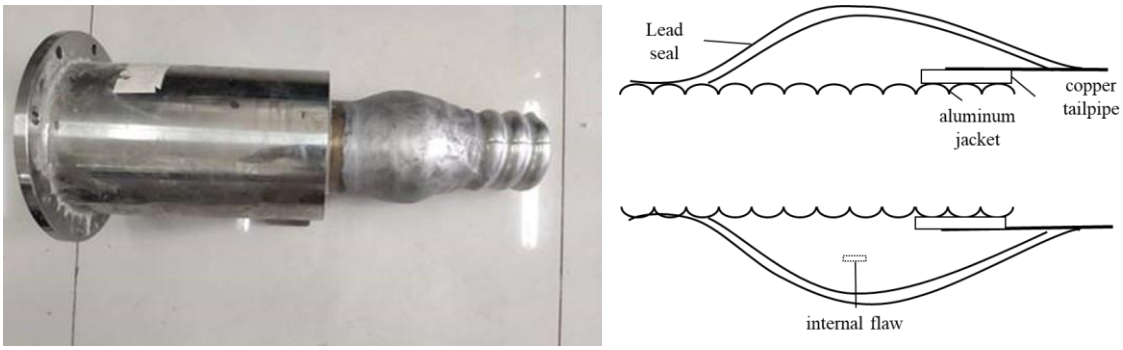

(a) Cable termination seals actual and defective schematic diagrams

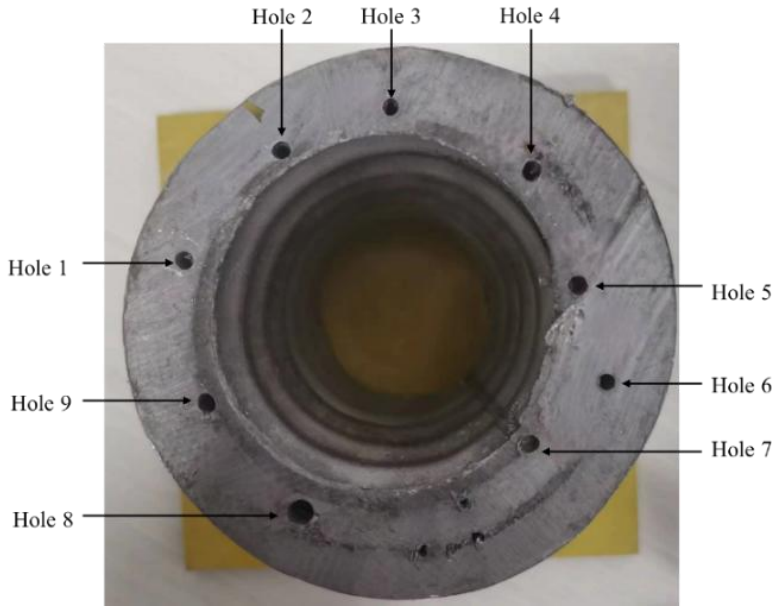

(b) Schematic diagram of manual defects in lead seals

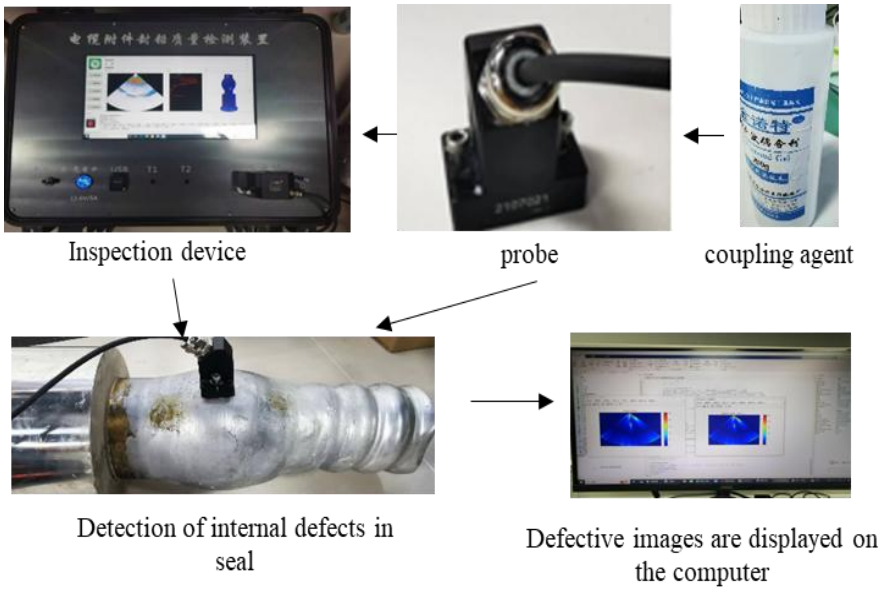

(c) Experimental platform for seal defect detection

Figure 4: Sample production and experimental platform construction for seal defects

4.2 Comparison of phased-array fan-scan imaging denoising methods for cable termination seals

Using the experimental platform shown in Figure 4(c), holes 1-9 of the lead seal artificially manufactured defects are detected separately, and the fan-scan images of the seal defects with very severe background noise are selected, which are the fan-scan images of holes 1, 2, and 3 of the seal with a radius of 3 mm, and the fan-scan image of hole 4 with a radius of 4 mm. The experimental detection results are shown in Figure 5(a), Figure 5(b), Figure 5(c), and Figure 5(d), respectively, and the background noise and artifacts in the following four figures are very easy to interfere with the technician's judgment of the seal defects.

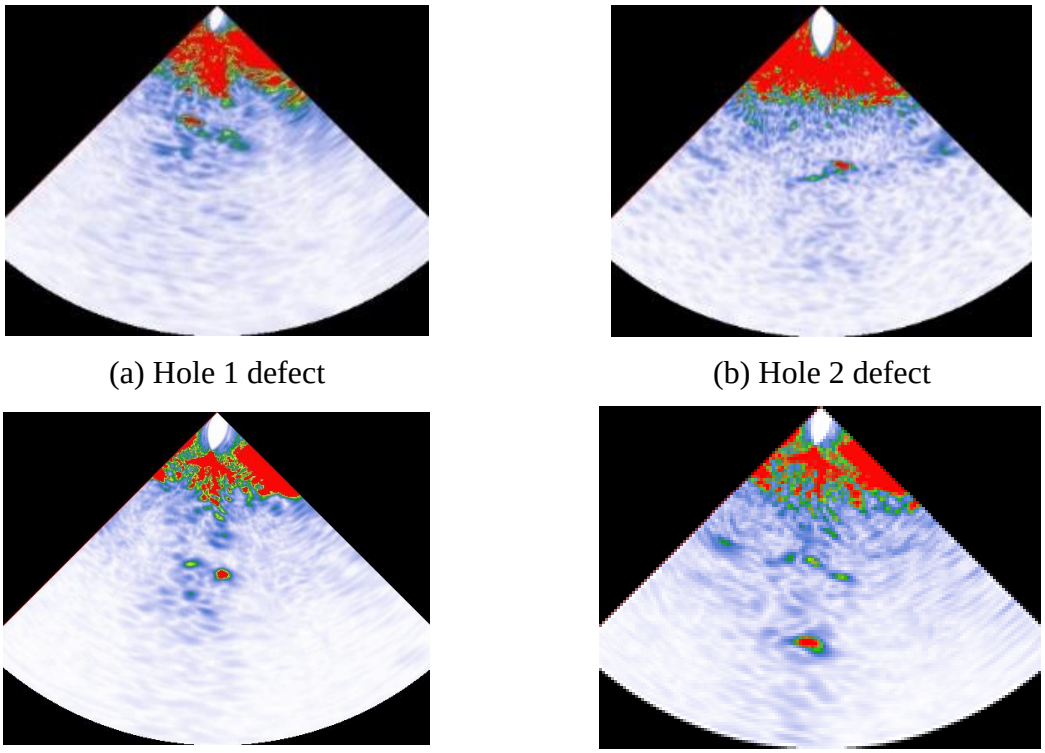

(a) Hole 1 defect (b) Hole 2 defect

(c) Hole 3 defect (d) Hole 4 defect

Figure 5: Experimental images of seal defects

Three filtering methods, median, mean and threshold, are used respectively to process the image data of different diameters of lead seal hole defects in Figure 5, and obtain the median filter denoising map in Figure 6, the mean filter denoising map in Figure 7, and the threshold filter denoising map in Figure 8.

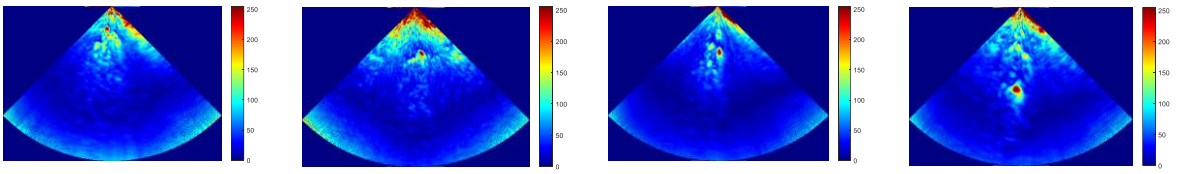

(a) Hole 1 defect (b) Hole 2 defect (c) Hole 3 defect (d) Hole 4 defect

Figure 6: Lead seal median filter denoising image

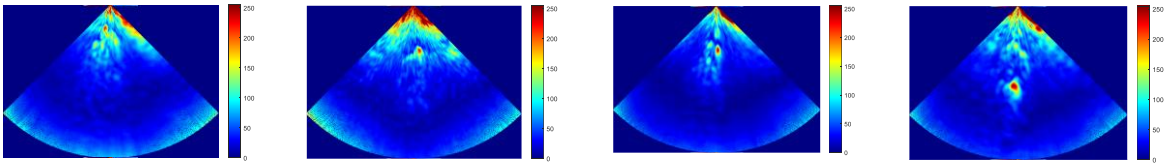

(a) Hole 1 defect (b) Hole 2 defect (c) Hole 3 defect (d) Hole 4 defect

Figure 7: Lead seal mean filter denoising image

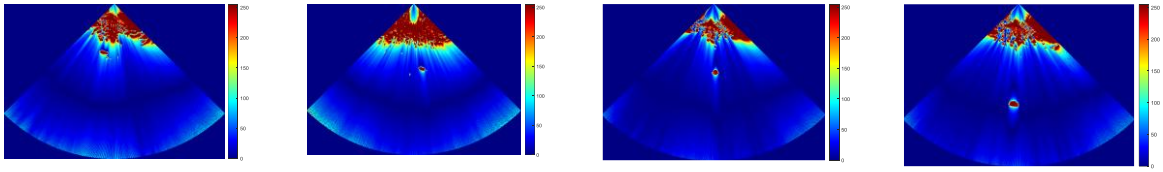

(a) Hole 1 defect (b) Hole 1 defect (c) Hole 3 defect (d) Hole 4 defect

Figure 8: Lead seal threshold filter denoising image

The median-filtered image of the four holes of the lead seal in Figure 6 is slightly improved over the noise and artifacts in Figure 4, while the continuity of the defect edges is poor. The mean-filtered image of the four holes in the lead seal in Figure 7 has less noise and artifacts than in Figure 4, while the clarity of the defect edges is reduced. The image of the four holes of the lead seal after threshold filtering in Figure 8 is clearer than the edge of the defects in Figure 4, and the noise and artifacts are significantly reduced, with high image resolution and signal-to-noise ratio, which can clearly reflect the size of the defects.

The above is an intuitive analysis of the filtered image of the lead seal defects, and next, in order to measure the degree of approximation between the fan-scanned image of the lead seal defects and the original image after denoising, the peak signal-to-noise ratio PSNR and the structural similarity SSIM can be used as the quantitative criterion for the evaluation of the image quality[18].

The peak signal-to-noise ratio is calculated as:

$$PSNR\left(Y,\hat{Y}\right)=10\lg\left(\frac{255^2}{MSE}\right) \tag{12}$$

where: $\hat{Y}$ is the estimated value of the signal Y, MSE is

$$MSE=\frac{1}{IJ}\sum_{i=1}^{I}\sum_{j=1}^{J}\left(Y_{i,j}-\hat{Y}_{i,j}\right)^2 \tag{13}$$

Where: I and J denote the length and width of the 2D signal, respectively.

The SSIM is calculated as:

$$SSIM\left(x,y\right)=\frac{\left(2\mu_x\mu_y+c_1\right)\left(2\sigma_{xy}+c_2\right)}{\left(\mu_x^2+\mu_y^2+c_1\right)\left(\sigma_x^2+\sigma_y^2+c_2\right)} \tag{14}$$

x and y are denoted as the denoised image data and original image data, respectively; μ_x and

μ_y are the means of x,y; σ_x^2 and σ_y^2 are the variances of x,y; σ_{xy} is the covariance of x,y; c_1 and c_2 are two constants.

Due to the inability of the ultrasound phased array probe and the system to detect defects and other information in the blind zone, which is the red area above the image in Figure 5, the blind zone is not considered here in the spirit of accurately quantifying the denoising ability of the three methods for fan-scanned images of lead seal defects. Here the raw image data is processed into data at the seal defects plus background noise free data. Therefore, after removing the image data from the blind area, the PSNR values of the fan-scan images of the defective holes in the lead seals 1, 2, 3, and 4 were calculated and processed by the three

denoising methods as shown in Table 2.

Table 2: Peak signal-to-noise ratio of fan-scan images of seal defects processed by four denoising methods /dB

Methods	Hole 1	Hole 2	Hole 3	Hole 4
median filter	18.7719	18.9290	23.5413	18.8240
mean value filter	18.9337	19.1595	23.7866	19.0252
threshold filtering	24.1454	26.2617	30.2955	24.4574

Source:
Table by author

The PSNR of the threshold filtering algorithm was on average 6.27dB and 6.06dB higher than the median and mean filters, respectively, under the four hole defects of the lead seal.

In the experiment, the diameter of the seal defects is 3mm and 4mm, and the SSIM of the fan-scan image of the seal defects is calculated in the region centered on the defects and drawn with a side length of 6mm, and the results are shown in Table 3.

Table 3: SSIM of fan-scan images of seal defects processed by four denoising methods /dB

Methods	Hole 1	Hole 2	Hole 3	Hole 4
median filter	0.5834	0.6374	0.7567	0.7361
mean value filter	0.5602	0.6260	0.7352	0.7245
threshold filter	0.6818	0.6870	0.7822	0.7523

Under the four hole defects of the lead seal, the SSIM of the threshold filtering algorithm was on average 0.05dB and 0.06dB higher than the median filter and the mean filter, respectively.

4.3 Comparison of results of processing steps for image quality optimization

In order to compare the effect of image data processing in imaging, threshold filtering with Lanczos interpolation was removed in two data processing for two imaging sessions. The imaging results are shown in Figure 9.

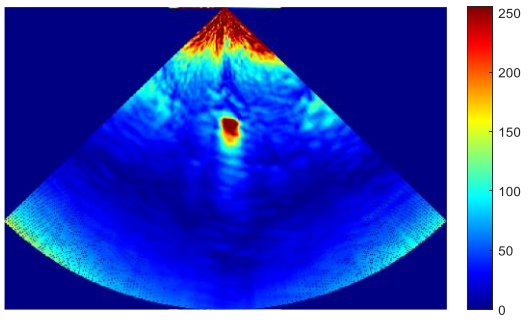

(a) Algorithmic imaging without threshold filtering

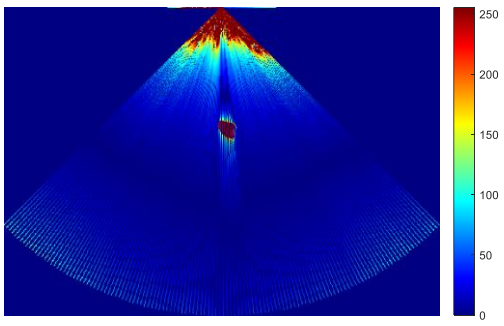

(b) Algorithmic imaging without Lanczos interpolation

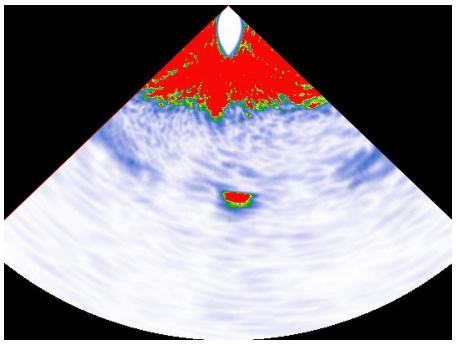

(c) original image

Figure 9: Image optimization processing comparison

In Figure 9(a), since the seal defect image data is not threshold filtered, the noise around the defect as well as the background noise still exists, and the shape of the defect is distorted, which will seriously interfere with the quantization of the size of the seal defect. In Figure 9(b), the seal defect image data without Lanczos interpolation, although the surrounding noise is removed, the inside of the defect is streaked and the edge of the defect is discontinuous, which also affects the judgment of the size of the seal.

5 Conclusion

In this study, an optimization method for lead seal fan-scan imaging is proposed, which processes the fan-scan image data of lead seal defects acquired by phased array equipment after imaging. The processing workflow consists of three main steps: first, filtering the image data; second, applying the Hilbert transform to extract the envelope; and finally, performing Lanczos interpolation. The processed images exhibit significantly reduced noise and artifacts, sharper defect edges, and improved resolution compared to the original data.

Experimental results demonstrate that when filtering the fan-scan image data of lead seal hole defects, the threshold filtering method achieves higher Peak Signal-to-Noise Ratio (PSNR) and Structural Similarity Index (SSIM) values compared to median and mean filtering. This approach effectively removes background noise and artifacts, enhances imaging quality, and preserves defect size information. Furthermore, Lanczos interpolation of the image data significantly improves the continuity of the edges of lead seal hole defects. This method holds practical application value for ultrasonic phased array detection of cable terminal lead seal defects and contributes to the accurate quantification of such defects.

Author Declarations

All authors promise that the article [Ultrasonic imaging optimization of cable lead seal defects based on filtering interpolation] has no conflicts to disclose.

Availability of data

The data that support the findings of this study are available from the corresponding author upon reasonable request.

References

[1] Cao J, Li N, Jiang P, et al. Research on eddy current testing technology for lead seal crack defects of high voltage cable[C]//2019 IEEE 3rd International Conference on Circuits, Systems and Devices (ICCSD). IEEE, 2019: 171-176.

[2] Caroline Holmes, Bruce W Drinkwater, Paul D. Advanced post-processing for scanned ultrasonic arrays: Application to defect detection and classification in non-destructive evaluation. Ultrasonics, 48 (2008) 636–642.

[3] Fang Chunhua, Hu Dongsan, Tao Yuning,et al. Ultrasonic phased array flexible coupling detection of lead seal defect in high voltage cable terminal[J]. High Voltage Engineering, 2022,48(01): 29-37.

[4] Fang Chunhua, Hu Dongsan, Tao Yuning,et al. Research on ultrasonic detection method of lead seal defects in high voltage cable terminal[J]. China Test, 2022, 48(03): 118-123.

[5] Guo C S,Han Y J,Xu J B. Radial Hilbert transform with Laguerre-Gaussian spatial filters[J]. Opt Lett, 2006, 31(10), 1394-1396.

[6] Hadi G, Hamid B, Jahan T. Toward high-intensity focused ultrasound lesion quantification using compressive sensing theory[J]. Journal of engineering in medicine. 2017, 231(12): 1152-1164.

[7] He H B, Sun K H, Sun C M, Jianguo He, Enfu Liang, Qian Liu, Suppressing artifacts in the total focusing method using the directivity of laser ultrasound[J]. Photoacoustics, 2023, 31(09): 100490.

[8] Kumar S, Menaka M, Venkatraman B. Simulation and experimental analysis of austenitic stainless steel weld joints using ultrasonic phased array[J]. Measurement Science and Technology, 2019, 31(2): 024005.

[9] Li Gang. Research on sector scanning imaging of ultrasonic phased array detection[D]. Xi’an:Xi’an University of Science and Technology, 2019.

[10] Ma Qiang, et al. Research on multi-physical field analysis and assessment technique of virtual connection defects in cluster cable joints based on digital twin technology. Frontiers in Energy Research. 12(2024): 1362361.

[11] Mou Xinong. Threshold Neighborhood Mean Based Denoising Algorithm for Medical Ultrasound Images[J]. Journal of Guizhou University(natural sciences edition), 2023, 40(01): 75-78.

[12] Otsu N. A Threshold Selection Method from Gray-Level Histograms[J]. IEEE Transactions on Systems Man & Cybernetics, 2007, 9(1): 62-66.

[13] Sikhakhane K, Rimer S, Gololo M, et al. Hybrid speckle de-noising filters for ultrasound images[C]//2023 IEEE AFRICON. IEEE, 2023: 1-6.

[14] Wei Y, Rui T, Li H, et al. Study on Noise Reduction Using a Wavelet Packet for Ultrasonic Flaw Detection Signal of a Small Diameter Steel Pipe with a Thick Wall[J].

International Journal of Acoustics and Vibrations, 2014, 19(3): 198-202.

[15] Xu J, Lu Z Y, Bian D, et al. Ultrasonic signal characterization of typical internal defects in silicone rubber for 10kV cable intermediate joint insulation[C]// 2023 3rd International Conference on New Energy and Power Engineering. Huzhou: IEEE, 2023: 346-351.

[16] Xu, Q, Wang H. Sound field modeling method and key imaging technology of an ultrasonic phased array: A review[J]. Applied Sciences, 2022,12(16): 7962.

[17] Yang Xiuqing. Iterative back projection image super-resolution algorithm based on Lanczos interpolation[D]. Shandong:Shandong University, 2018.

[18] Zhou Y, Yu M, Ma H, et al. Weighted-to-spherically-uniform SSIM objective quality evaluation for panoramic video[C]. 2018 14th IEEE International Conference on Signal Processing (ICSP), Beijing, 2018: 54-57.

[19] Zhang X,Zuo G,Memon SA, et al. Effects of initial defects within mortar cover on corrosion of steel and cracking of cover using X-ray computed tomography. Construction and Building Materials. 223(2019): 265-277.

[20] Zhong S, Zhong J, Zhang Q, et al. Quasi-optical coherence vibration tomography technique for damage detection in beam-like structures based on auxiliary mass induced frequency shift[J]. Mechanical Systems & Signal Processing, 2017, 93(Sep.): 241-254.